*aerospace*

MDPI

*Article*

# Development of a Global Model for the Analysis of Plasma in an Atmosphere-Breathing Cathode-Less Thruster

**Simone Dalle Fabbriche [1,*], Nabil Souhair [1], Mirko Magarotto [2], Raoul Andriulli [1], Enrico Corti [1] and Fabrizio Ponti [1]**

[1] Alma Propulsion Laboratory, Department of Industrial Engineering (DIN), University of Bologna, 40126 Bologna, Italy; nabil.souhair2@unibo.it (N.S.); raoul.andriulli@unibo.it (R.A.); fabrizio.ponti@unibo.it (F.P.)
[2] Department of Information Engineering (DEI), Univeristy of Padova, 35122 Padua, Italy; mirko.magarotto@unipd.it
* Correspondence: simon.dallefabbriche@studio.unibo.it

**Abstract:** This study investigates the preliminary propulsive performances of a cathode-less plasma thruster with air as its propellant. The analysis is carried out through a global model and simulates a thruster over a power range of 0 to 50 W. The developed code considers a set of 177 chemical reactions involving 8 different species and includes empirical equations to account for electronegative effects. The analysis presents the steady-state values of species densities at 10 W, 30 W, and 50 W to gain insights into the key characteristics of plasma dynamics. Moreover, the study estimates the thrust and specific impulse and compares the results to data from models that employ xenon and iodine, aiming to understand the performances of air in low-power thrusters. Lastly, the study examines the effects of varying air inflow concentration on the chemistry, analyzing three different orbit altitudes (i.e., 200, 300, and 400 km).

**Keywords:** aerospace propulsion; numerical modeling; plasma thruster; atmosphere breathing electric propulsion; global model; plasma chemistry model



**Citation:** Dalle Fabbriche, S.; Souhair, N.; Magarotto, M.; Andriulli, R.; Cort, E.; Ponti, F. Development of a Global Model for the Analysis of Plasma in an Atmosphere-Breathing, Cathode-Less Thruster. *Aerospace* **2023**, *10*, 389. https://doi.org/10.3390/aerospace10050389

Academic Editor: Sergey Leonov

Received: 22 March 2023
Revised: 8 April 2023
Accepted: 19 April 2023
Published: 23 April 2023



## 1. Introduction

In the field of space technology, there are numerous uses that require satellites to be positioned in low orbits. This area is particularly important for applications such as communication and Earth observation, where performance is directly influenced by the distance from the target [1]. For this reason, its not surprising that the most crowded region around the Earth is the low Earth orbit (LEO) zone, ranging from 260 to 2000 km [2]. However, greater benefits can be obtained by positioning the satellites into the lower part of LEO, which is called the very low Earth orbit (VLEO) and refers to the region below 450 km [3,4].

VLEO is a desirable region for satellite applications due to its proximity to the Earth and lower launch costs. Reaching a lower orbit is indeed less demanding in terms of the $\delta$v required, thus saving on propellant and downsizing the launcher vehicles [5]. Moreover, VLEOs are located in a part of the thermosphere which is not so well-characterized, making the region also desirable for scientific purposes. However, this zone represents a very challenging band due to the presence of a residual atmosphere with higher density, thus a stronger effect is produced by atmospheric drag. In particular, this force has a great influence on the spacecraft, reducing the orbital velocity and leaving the satellite to drop in a way that is not compatible with the typical satellite's operative lifetime [6]. To mitigate the spacecraft's orbital decline, a drag compensation system is needed. Since the requirements are very demanding in terms of stored and consumed propellant, electric propulsion systems are the best option for this purpose due to their high specific impulse [7]. However,

even in this case, the spacecraft's design must foresee a consistent amount of propellant that can only be used for drag compensation.

Atmosphere-breathing electric propulsion systems (ABEP) have been proposed to accomplish this purpose. The concept consists of using the residual air present in the VLEO space atmosphere as a propellant for an electric thruster instead of the commonly used noble gases [8]. These gases can be indeed ionized and accelerated by electric fields to generate thrust. Even though performances are in theory lower than the most commonly used xenon or iodine [9], ABEP systems are considered promising for their potential to reduce the masses of spacecrafts and make missions more cost-effective, as they eliminate the need to carry heavy fuel loads. Moreover, the absence of a limited storage of propellant makes this technology a good candidate for atmospheric drag compensation since it has a theoretically infinite propulsive lifetime [10].

In the VLEO region, the atmosphere is mainly composed by oxygen and nitrogen, both in atomic and molecular form [11], but the mixture of gases is not constant and changes with the altitude, which makes it difficult to predict thruster characteristics. Moreover, even in this case, there is a significant corrosive effect from the generated particles [12]; thus, materials need to be accurately selected. Therefore, cathode-less thrusters such as the Helicon plasma thruster (HPT) are favored over other types of thrusters as they have smaller surfaces exposed to the corrosive flow. However, the thrust efficiency of these thrusters can reach values around 30% [13], which is lower than that of other mature systems such as Hall effect thrusters and ion gridded thrusters. Nevertheless, the presence of residual atmosphere can be an advantage in terms of spacecraft security since space debris would degrade more quickly, decreasing the possibility of catastrophic impacts with foreign objects [14].

Several ABEP projects have been studied in the last few years. For example, ESA is developing the project RAM-EP (Residual Atmosphere for Maneuvering by Electric Propulsion) [15], which consists of an atmosphere-breathing electric propulsion system that aims to demonstrate the feasibility of using the residual atmosphere as a propellant for electric thrusters in VLEO. Similarly, the Japanese Aerospace Exploration Agency (JAXA) is working on their project, the ABIE (Air-Breathing Ion Engine) [16]. The goal of the program is to improve the efficiency and performances of electric propulsion systems by using residual atmospheric air as a propellant. Recently, the European Commission founded the project AETHER (Atmosphere-breathing Electric THrustER) [17] to demonstrate the sufficient and reliable net thrust production of an ABEP system for a sustained period of time. In addition, the privately owned space propulsion company Busek Co. (Natick, MA, USA) is working on its own atmosphere-breathing electric propulsion system. The project, called the Martian Atmosphere-Breathing Hall Effect Thruster (MABHET) [18], is the first approaching the use of an ABEP system in a Martian environment. The intention is to demonstrate that it is possible to use atmosphere-breathing systems for planetary exploration, reducing the amount of heavy propellant needed by the spacecraft and making it more efficient and cost-effective for long-duration missions on Mars.

Finally, at Stuttgart University, a group of researchers has presented the DISCOVERER project [19,20] for a Helicon-based plasma thruster, which aims to use ABEP technology for long-term remote sensing operations in VLEO.

In order to provide a preliminary overview of thruster performances and to optimize the design of ABEP models, simulations of atmosphere plasma must be carried out. In particular, Taploo et al. have studied the chemistry of an atmosphere-breathing system in a range from 80 to 110 km by varying the mean electron energy with a consistent set of considered reactions [11]. Moreover, the project aims to present an ABEP design without an external neutralizer. A global model (GM) for zero-dimensional simulations is presented by Mrozek et al. [21], which simulates a gridded atmosphere-breathing electric propulsion system with a high-frequency plasma source. The model was validated using experimental measurements in a pressure range from from $10^{-3}$ Pa to 1 Pa, and the focus was on investigating the scalability of the plasma source.

There are also some works in the literature related to multi-dimensional models. In particular, Zhou et al. [9] developed a fluid two-dimensional asymmetric code to provide preliminary results for an atmosphere-breathing Helicon plasma thruster (HPT) and compares the propulsive performances to a xenon fed HPT. Another fully kinetic multi-dimensional model has been studied by Taccogna et al. [22] to analyze possible changes in size-geometry, electrode arrangement, and magnetic field topology, aiming to optimize the efficiency of the mass propellant's utilization in an ABEP thruster.

This study uses three different global models to analyze the preliminary performances of a cathode-less thruster with a power range of up to 50 W, e.g., the Helicon plasma thruster REGULUS-50 developed by the Italian company Technology for Propulsion and Innovation (T4i) [23,24]. The models simulate a range of propellants, including traditional gases such as xenon and alternative options such as iodine and air, with a particular focus on the chemistry models. The objective of the study is to understand the relative behavior of different gases and the main characteristics of air used on these systems. Additionally, air-fed simulations account for the predicted inflow at various orbits, taking into consideration the consistent variation in species concentrations and atmospheric pressure with changes in altitude.

## 2. Methodology

Global models analyze the time evolution of plasma in a 0-dimensional domain, hence without direct consideration of spatial variations, which makes them computationally efficient.

Figure 1 presents the scheme of an atmosphere-breathing, cathode-less, RF plasma thruster, which includes an intake and a cylindrical ionization chamber terminating with an open section, where ions are accelerated by a magnetic nozzle. Plasma is produced and confined inside the cylinder with radius $R$ and length $L$. The magnetic field is uniform and aligned with the thruster's axis, but cusps are considered through empirical equations [25].

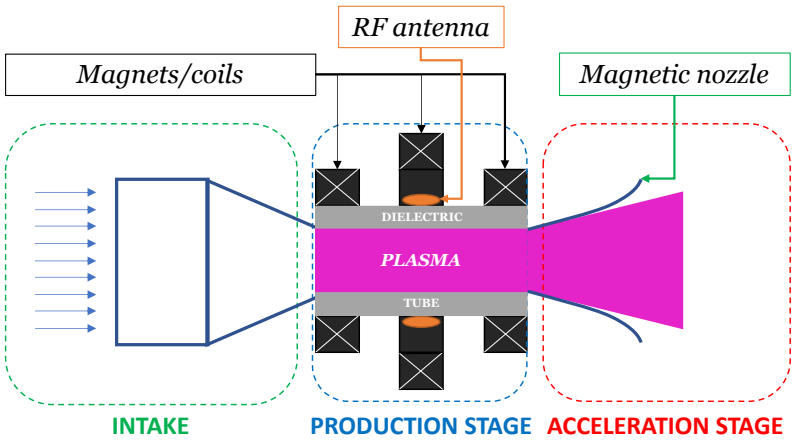


**Figure 1.** Atmosphere-breathing, cathode-less plasma thruster layout.

The set of governing equations counts one particle balance equation for each species that has been considered, and the electron power balance is obtained by the Ordinary Differential Equation (ODE ) [26–28]:

$$\frac{\mathrm{d}n_i}{\mathrm{dt}} = \Psi_i + \Psi_{\mathrm{wall}_i} + \Psi_{\mathrm{in}_i} - \Psi_{\mathrm{exh}_i} \tag{1}$$

$$\frac{\mathrm{d}}{\mathrm{dt}}\left(\frac{3}{2} n_e k_\mathrm{B} T_e\right) = P_\mathrm{w} - P_\mathrm{chem} - \Psi_\mathrm{wall}\varepsilon_\mathrm{wall} - \Psi_\mathrm{exh}\varepsilon_\mathrm{exh} \tag{2}$$

Here, $n_i$ is the number density of the generic i-th species. $\Psi_\mathrm{in}$ and $\Psi_{\mathrm{exh}_i}$ are the entering and exiting particle flows, respectively, while $\Psi_i$ and $\Psi_{\mathrm{wall}_i}$ are source terms that contain i-th's production and loss by volume and surface reactions. In the second equation, $n_e$ is the

electron particle density, $k_B$ is the Boltzmann's constant, and $T_e$ is the electron temperature expressed in [eV]. $P_w$ is the uniform power density deposited by the antenna to electrons, and $P_{chem}$ is the source/sink term associated with plasma reactions. $\Psi_{wall}\varepsilon_{wall}$ and $\Psi_{exh}\varepsilon_{exh}$ are the wall and exhaust power losses, respectively, obtained by multiplying the particle's flow by the associated energy. The populating and depopulating mechanisms for a generic species $i$ can be expressed by the following equation:

$$\Psi_i = \sum_{j_1 \neq j_2} n_{j_1} n_{j_2} K_{j_1 j_2 i} \tag{3}$$

where $n_{j_1}$ and $n_{j_2}$ are the densities of the two generic reactants, while $K_{j_1 j_2 i}$ is the reaction rate of the reaction that involves both reactants and product $i$. Similarly to the particle balance, the source/sink terms in the power balance can also be evaluated by the use of the reaction rates. Since the power balance solely addresses electron energy, only electron–heavy particle interactions are considered, i.e.,

$$P_{chem} = \sum_j \sum_i n_e n_j K_{ji} \varepsilon_{ji} \tag{4}$$

where $\varepsilon_{ji}$ is the energy lost or released for the generic $j \rightarrow i$ reaction and is given in [eV]. In case of elastic scattering interaction, i.e., when both $j$ and $i$ species are equal, the value of this parameter can be evaluated as $3\frac{m_e}{m_i}T_e$ [29], where $m_e$ and $m_i$ are the electron mass and the mass of species $i$, respectively. The sink term for surface reactions $\Psi_{wall_i}$ in the particle balance of the generic $i-th$ species can be determined as:

$$\Psi_{wall_i} = \Gamma_{wall_i} \frac{A_{eff}}{V} = n_i u_{B_i} \frac{A_{eff}}{V} \tag{5}$$

Here, $\Gamma_{wall_i}$ is the flux of the i-th species and $V$ is the chamber volume. Moreover, $u_{B_i}$ is the Bohm speed and $A_{eff}$ represents the effective area, i.e., the wall area affected by surface losses [30]. While positive ions are governed by Equation (5), electron losses are obtained with the hypotheses of quasi-neutrality; thus, the number of lost electrons is equal to the number of lost positive ions. In order to evaluate the energy lost at the wall, the number of recombined electrons has to be multiplied by the term $\varepsilon_{wall}$, which can be expressed as:

$$\varepsilon_{wall} = 2T_e - \frac{T_e}{2} \ln\left(\frac{2\pi m_e}{m_i}\right). \tag{6}$$

The exhaust contribution for positively charged particles is provided by the term $\dot{m}_{out}$ in Equation (2). For the generic species $i$, this term can be computed as:

$$\Psi_{exh_i} = \Gamma_{exh} \frac{A_{exh}}{V} = n_i u_{B_i} \frac{A_{exh}}{V} \tag{7}$$

Here, $A_{exh}$ is the exhaust section. Exhausted neutrals are taken into account considering a free-molecular regime; hence, $\Gamma_g = 1/4 n_g u_{th}$, where $u_{th}$ and $n_g$ are the neutrals' thermal speed and number density [31]. Power losses due to exhaust are considered by multiplying the electron flux by the energy associated with each electron leaving the chamber [29], i.e.,

$$\varepsilon_{exh} = 2T_e - \frac{T_e}{2} \ln\left(\frac{2\pi m_e}{m_i}\right) \tag{8}$$

The effective area $A_{eff}$ was evaluated considering the presence of a non-uniform magnetic field (i.e., with cusps):

$$A_{eff} = 2\pi R^2 h_L \beta + h_{R\perp}(2\pi RL - A_{cusp}) + h_{R\parallel} A_{cusp} \tag{9}$$

where semi-empirical coefficients $h_R$, $h_L$, and $\beta$ are used to consider the non-uniformity of plasma profiles inside the source tube and the impact of electronegativity on diffusion coefficients [32]. $R$ and $L$ are the radius and the length of the cylindrical chamber, respectively, while $A_{cusp}$ is the total cusp area and can be evaluated as follows[25]:

$$A_{cusp} = 4N_{cusps}\sqrt{r_{ci}r_{ce}}2\pi R \tag{10}$$

where $r_{ci}$ and $r_{ce}$ represent the ion and electron cyclotron radii, i.e., the ratio between thermal velocity and cyclotron frequency. $N_{cusps}$ is the number of cusps and is set equal to 2 in this work. The equations mentioned are part of a global model that assumes the presence of only neutral and positively charged particles, such as in the case of a noble gas GM. However, when propellants like iodine and air are used, the presence of negatively charged particles can have a significant impact on the overall properties of the plasma. In such cases, the plasma tends to stratify into an electronegative core and an electropositive edge, as explained in [29]. To account for this behavior, certain parameters need to be corrected. In particular, the expression of $h_L$ and $h_R$ shall be [21,33]:

$$h_L = 0.86\left(3 + \frac{L}{2\lambda} + (1+\alpha)^{1/2}\frac{\gamma_+}{5}\left(\frac{L}{\lambda}\right)^2\right)^{-1/2}\left(\frac{\gamma_- - 1}{\gamma_-(1+\alpha)^2} + \frac{1}{\gamma_-}\right)^{1/2} \tag{11}$$

$$h_R = 0.8f_b\left(4 + \frac{R}{\lambda} + (1+\alpha)^{1/2}\gamma_+\left(\frac{R}{\lambda}\right)^2\right)^{-1/2}\left(\frac{\gamma_- - 1}{\gamma_-(1+\alpha)^2} + \frac{1}{\gamma_-}\right)^{1/2} \tag{12}$$

where $\alpha = n_-/n_e$ is the electronegativity parameter calculated in the bulk, while $\gamma_+$ and $\gamma_-$ are the temperature ratios described as:

$$\gamma_+ = T_+/T_e \tag{13}$$

$$\gamma_- = T_e/T_- \tag{14}$$

where $\lambda$ is the mean free path and $f_b$ is function of cyclotron frequency $\omega$ and mean free time $\tau$, as depicted by the equation:

$$f_b = (1 + (\omega\tau)^2)^{-1} \tag{15}$$

Negative ions are not considered in the exhaust flow since they are confined in the core, but the electronegative condition affects the power lost at the boundaries [29]. An equation for electronegative plasma has been introduced by [34], who defined the energy lost as:

$$\varepsilon_{wall} = 2T_e + qV_s + qV_p \tag{16}$$

where $q$ represents the charge of an electron, while $V_s$ and $V_p$ denote the magnitudes of the sheath voltage and plasma potential, respectively. The last two terms can be computed with the formulas provided by Thorsteinsson and Gudmundsson [35]:

$$V_p = \frac{T_e}{2}\frac{1+\alpha_s}{1+\gamma_-\alpha_s} \tag{17}$$

$$V_s = T_e\ln\left(4\frac{\langle\tilde{u}_B\rangle}{v_{th_e}}\frac{1+\alpha_s}{1+\alpha_s(v_{th_-}/v_{th_e})^2}\right). \tag{18}$$

where $v_{th_-}$ and $v_{th_e}$ refer to the thermal velocities of negative ions and electrons, respectively. The quantity $\langle \tilde{u}_B \rangle$ denotes the weighted average Bohm speed in electronegative conditions, which is determined as:

$$\tilde{u}_B = u_B \sqrt{\frac{1+\alpha_s}{1+\gamma_- \alpha_s}} \tag{19}$$

Finally, the electronegativity at the sheath edge $\alpha_s$ can be obtained solving the following equation:

$$\alpha_s = \alpha \exp\left(\frac{V_p}{T_e}(1-\gamma_-)\right) \tag{20}$$

Moreover, since plasma potential $V_p$ is itself a function of $\alpha_s$, the system is non-linear and is solved by a numerical approach. The use of molecular propellants also requires the recombination at the wall to be considered. This reaction is accounted for by:

$$\Psi_{wall_n} = \gamma_{rec} \Gamma_{th_n} \frac{A}{V} = \frac{1}{4} \gamma_{rec} n_n v_{th_n} \frac{A}{V} \tag{21}$$

where $\gamma_{rec}$ is the recombination coefficient and express the percentage of neutral atoms that recombine into molecules when hitting the wall, $\Gamma_{th_n}$ is the thermal flux for the generic n-species and $A$ is the total surface area. To calculate the diffusion parameters for a plasma containing molecules such as iodine and air, the Lennard-Jones potential method is used to empirically describe the interactions between the particles [36]. However, when dealing with molecular plasmas, a mixture-averaged approach must be considered to accurately compute the diffusion coefficient $D$ for each species $i$ in the mixture, i.e.,

$$D_i = \frac{1 - Y_i}{\sum_{j \neq i} \frac{X_i}{D_{ij}}} \tag{22}$$

where $X$ and $Y$ are respectively defined by:

$$X_i = \frac{n_i}{\sum n_j} \tag{23}$$

$$Y_i = \frac{m_i n_i}{\sum M_j n_j} \tag{24}$$

### *2.1. Chemistry Model*

It is crucial to provide a detailed explanation of the chemical models involved, as different propellants have distinct chemical properties. In this study, different types of thrusters were utilized to compare their propulsive performances with different propellants. The chemistry models for iodine and xenon are described in detail in [7,37], respectively. Air, instead, is a mixture of various gases, and its composition varies with the altitude. Therefore, certain reactions may become more or less relevant if the thruster is operated at different altitudes. The density evolution of oxygen and nitrogen in both atomic (O, N) and molecular ($O_2$, $N_2$) states with respect to orbit altitude is presented in Figure 2. The data have been computed using the MSIS-E-90 Atmosphere Model [38] at latitude 38.91 and longitude 77.04. These elements constitute the primary components of air, which is the inflow gas of the thruster. Nevertheless, other components may be generated within the ionization chamber due to collisions with heavy particles; hence, molecules such as nitric oxide (NO), nitrogen dioxide ($NO_2$), and nitrous oxide ($N_2O$) have been considered in the model to understand their contribution to the performances. The model developed considers a total of 8 different species (i.e., electrons, N, $N_2$, O, $O_2$, NO, $N_2O$, $NO_2$) and 177 chemical reactions, including elastic scattering, ionization, neutralization, and dissociation that are summarized in Table A1 in Appendix A. The code also takes into account heavy particle collisions, and considers negative ions during electron detachment and attachment

processes by means of a characteristic reaction rate $K_{ji}$ [9,11]. For reactions that involve electrons, the reaction rate is evaluated using the following equation:

$$K = \sqrt{\frac{2q}{m_e}} \int_0^\infty \varepsilon \sigma f_0 d\varepsilon \tag{25}$$

where $\varepsilon$ is the electron energy in electron-volts (eV), and $\sigma$ is the collision cross-section for the electron–particle reaction in meters squared ($m^2$). The electron energy distribution function (EEDF) $f_0$ is assumed to follow a Maxwellian distribution [39], given by:

$$f_0(\varepsilon) = 2\sqrt{\left(\frac{1}{T_e^3 \pi}\right)} \exp\left(-\frac{\varepsilon}{T_e}\right) \tag{26}$$

In this work, each species is considered in the ground state and with positively and negatively charged ions, except for nitrogen in both atomic and molecular forms due to its weak electronegativity, which makes negative ions unstable. Excited particles are supposed to rapidly decay into ground state through radiation emissions [40] and hence are not present as reactants but only as energy sink terms.

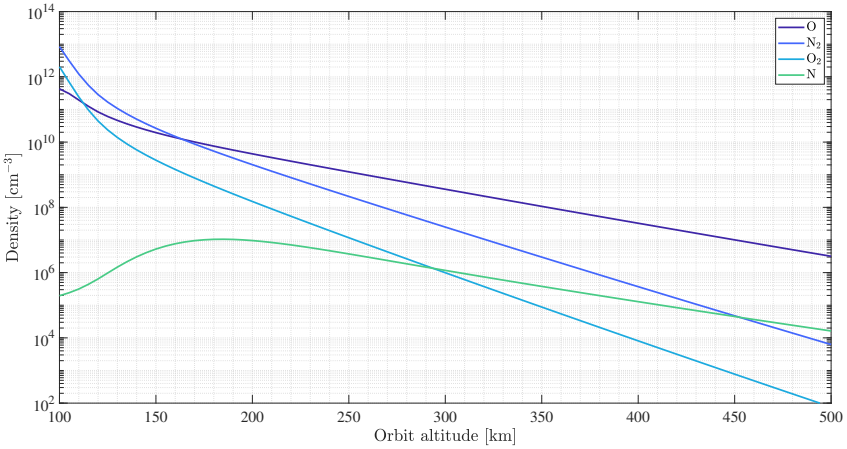


**Figure 2.** density of air species with respect to the orbit altitude.

### *2.2. Thrust Model*

The global model implements a thrust model to preliminary predict thrust $F$ and specific impulse $I_{sp}$, based on the plume model described in [41]. To make these predictions, certain assumptions are taken into account: (i) electron inertia is considered to be negligible; (ii) the cold ions hypothesis [42,43] is applied; and (iii) ions and electrons are assumed to exit the ionization chamber at the Bohm's speed ($u_B$). The total thrust is considered as being made up of two contributions, one provided by accelerated ions $F_p$ and the other by neutral expansion $F_{gas}$:

$$F = \sum_i \left(F_p^i + F_{gas}^i\right) \tag{27}$$

where $i$ indicates a generic species. The contribution of the neutrals to the thrust can be determined using the following equation:

$$F_{gas}^i = p_0^i A_{throat} \tag{28}$$

where $A_{throat}$ represents the throat section of the thruster, and $p_0^i$ is the fraction of the total pressure in the chamber related to the $i$-th species. Specifically, $p_0^i$ can be calculated as $p_0^i = k_B T_g n_{tot} X_i$, where $T_g$ is the neutral gas temperature and $n_{tot}$ is the total particle density of the neutral species. To evaluate the plasma contribution to the overall thrust,

both the source and magnetic nozzle effects are taken into account. These two effects are related if the assumption of paraxial approximation is valid for the magnetic nozzle, and this relationship is expressed by the following equation:

$$F^I_{\text{mag}} = F^I_0 \frac{(\mathcal{M}-1)^2}{2\mathcal{M}} \tag{29}$$

Here, $\mathcal{M}$ represents the magnetic Mach number, which is defined as the ratio of the plasma velocity $v$ to the Bohm's speed $u_B$. $F^i_0 = 2q\beta n^i_0 T_e A$ is the upstream plasma thrust, as defined in [41]. The overall contribution of the plasma to the thrust can be expressed as [44]:

$$F^I_{\text{p}} = F^I_0 \frac{\mathcal{M}^2_{\text{det}}+1}{2\mathcal{M}_{\text{det}}} \tag{30}$$

where the $\mathcal{M}_{\text{det}}$ is determined according to [41]. Finally, the specific impulse is evaluated using the following equation [45]:

$$I_{\text{sp}} = \frac{F}{g_e \dot{m}_0} \tag{31}$$

where $g_e$ represents the gravity acceleration constant at sea level and $\dot{m}_0$ is the total mass flow rate.

## 3. Results

In this section, the results of an investigation into the use of air propellant applied to cathode-less thrusters are presented. In order to analyze the main characteristics and differences, the propulsive performances associated with these propellants are compared via simulations carried out with the global model described in Section 2. Additionally, three different orbital conditions are considered for the air case, which are at altitudes of 200 km, 300 km, and 400 km. These conditions are simulated to represent the varying atmospheric compositions that the thruster would encounter when operating at different orbit altitudes. It is important to note that, while the GM results for xenon and iodine propellant systems have been validated against empirical data [46–48], there are currently limited experimental data available in the literature to validate results for cathode-less thrusters fed with air [49]. Furthermore, the few measurements available are not representative of the conditions considered in this work, particularly for different orbit altitudes. The comparison between the global models is carried out by evaluating the physical characteristics of a thruster with a cylindrical chamber that has a length (L) of 80 mm and a radius (R) of 7.5 mm. The magnetic field strength is set to 0.06 T, and it is assumed that the inflow rate remains constant at 0.1 mg/s. However, it should be noted that this hypothesis may not be valid for air, as the mass flow rate is dependent on the orbit altitude. Nonetheless, this study is focused on comparing the chemistry effects in different global models, and for this reason, the value is being considered as constant. As a preliminary step, the air model has been simulated with three different input power levels (i.e., 10 W, 30 W, and 50 W) for each of the three orbits. The resulting steady-state values for ion species densities in units of [$m^{-3}$] are shown in Figures 3–5. Overall, the simulations exhibit a common feature: the population of negative ions is at least two orders of magnitude lower than that of positive ions, indicating a weakly electronegative plasma. Additionally, the quasi-neutrality principle is upheld, as the number of positively charged particles is in close proximity to that of the negative ones. Furthermore, the results reveal that the primary positive ions are $O^+$, while nitrogen, in both atomic and molecular forms, is present in lower concentrations. This gap increases with orbit altitude, in accordance with the data from Figure 2. Notably, the sum of positive ions is almost equal in all the three considered orbit altitudes, but the lowest case exhibits a higher population of molecular ions. Finally, the density of molecules, such as $NO^+$, $N_2O^+$, and $NO^+_2$ is several orders of magnitude lower than other species; hence, their effect is not relevant in the behavior of the system.

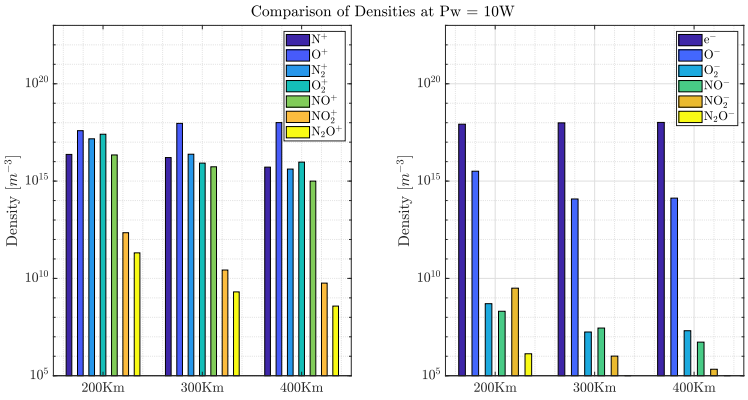


**Figure 3.** Steady-state density values for global air model with 10 W input power.

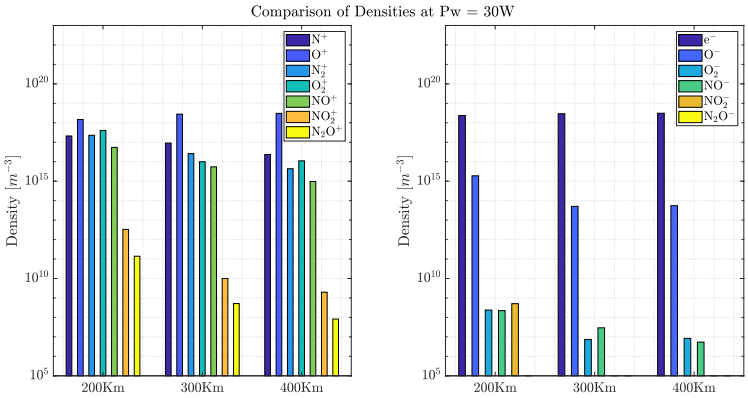


**Figure 4.** Steady-state density values for global air model with 30 W input power.

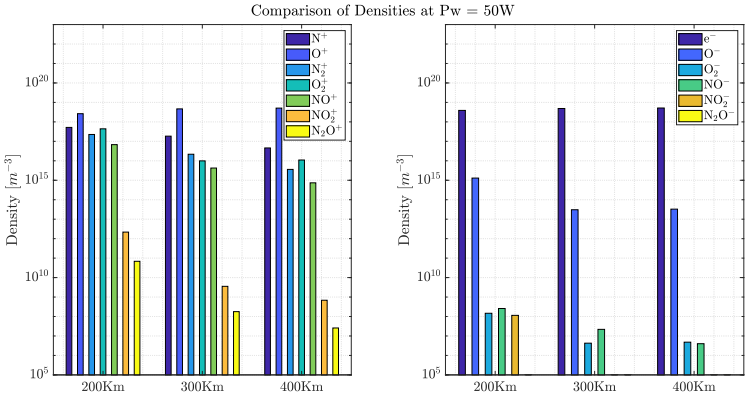


**Figure 5.** Steady-state density values for global air model with 50 W input power.

Based on the methodology described in Section 2, the propulsive performances of three different global models have been estimated, and the results are presented in Figure 6. The thrust and specific impulse values of these models are plotted as a function of the input power, and the performances of air at 300 km altitude is compared against the numerical results for the other two propellants. The plot also includes empirical measurements from REGULUS-50 using both iodine and xenon and demonstrates the agreement with simulated values within the error bands, which have been assumed at 25% for the global models.

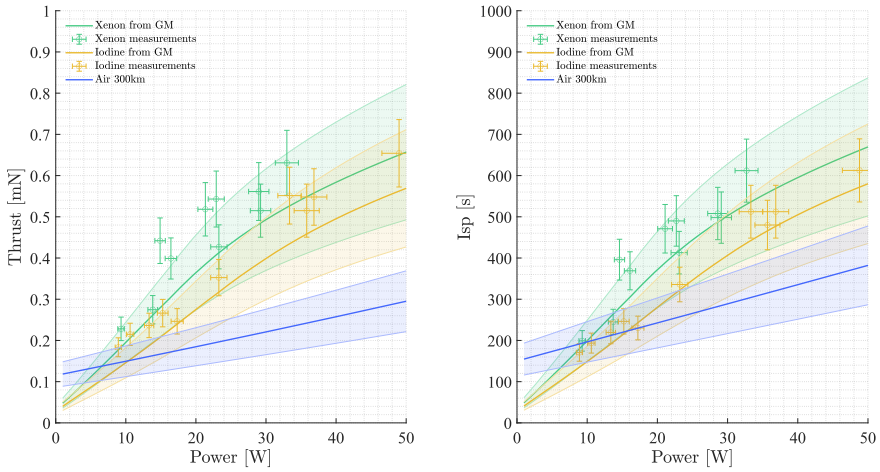


**Figure 6.** Comparison of thrust and specific impulse values obtained from the different propellants with respect to the input power in range 0–50 W.

It is evident from the plots that air has poor propulsive performances with respect to xenon and iodine. At 50 W input power, the air case presents less than 50% of the thrust and specific impulse in relation to xenon and iodine. This condition is caused by the fact that, with this low input power, air is fundamentally not ionized. Indeed, most of the energy introduced into the system is lost in molecular dissociation processes, resulting in high losses. Additionally, the ionization potential required for nitrogen and oxygen is higher than that for xenon and iodine [50]; hence, more energy is necessary to produce a singly ionized particle. Furthermore, air has a lower molecular mass compared to xenon and iodine. Consequently, for the same mass flow rate, a larger number of elementary particles is injected into the system, requiring more ionization events to achieve full ionization.

Table 1 illustrates the different ionization ratios (i.e., the ratio between the sum of positive ions and all particles) of air at 300 km with respect to three different input powers. The table also highlights the densities of positively charged particles and electrons at 50, 300, and 700 W. Even if increasing the power in a system designed for 50 W does not have a physical meaning, the table mentioned clarifies the behavior of the air propellant in cathode-less thrusters. As previously explained, the poor thrust and specific impulse values are consequences of a weakly ionized gas. The ionization ratio at 50 W indicates that less than the 8% of the overall particles have been ionized. This value is very low if compared against Table 2, where xenon and iodine results at 50W input power are presented.In both high-energy cases, instead, the density of positive ions is more than 50% of the total amount. In particular, in order to achieve a significant ionization percentage, the input power has to be much higher than the analyzed range.

**Table 1.** Ionization ratio, electron density, and positive ion density steady-state values for different input powers using air.

| Quantity | 50 W | 300 W | 700 W |
|---|---|---|---|
| Ionization Ratio | $7.55 \times 10^{-2}$ | $5.57 \times 10^{-1}$ | $7.61 \times 10^{-1}$ |
| Electron density [$m^{-3}$] | $4.87 \times 10^{18}$ | $2.54 \times 10^{19}$ | $2.26 \times 10^{19}$ |
| Positive ion density [$m^{-3}$] | $4.87 \times 10^{18}$ | $2.54 \times 10^{19}$ | $2.26 \times 10^{19}$ |
| Neutral density [$m^{-3}$] | $5.96 \times 10^{19}$ | $2.02 \times 10^{19}$ | $7.09 \times 10^{18}$ |

**Table 2.** Ionization ratio, electron density, and positive ion density steady-state values in the xenon and iodine cases at 50 W input power.

| Quantity | Xenon | Iodine |
|---|---|---|
| Ionization Ratio | $8.86 \times 10^{-1}$ | $9.3 \times 10^{-1}$ |
| Electron density [$m^{-3}$] | $9.43 \times 10^{18}$ | $1.20 \times 10^{19}$ |
| Positive ion density [$m^{-3}$] | $9.43 \times 10^{18}$ | $1.20 \times 10^{19}$ |
| Neutral density [$m^{-3}$] | $1.23 \times 10^{18}$ | $1.94 \times 10^{18}$ |

Finally, Figure 7 presents an investigation on the influence of orbit altitude on propulsive performances. The plots illustrate the thrust and $I_{sp}$ results for three different inflow concentrations, representing 200, 300, and 400 km across a power range from 0 up to 300 W. Overall, the trends observed for the different propellants are very similar, and any differences between the values are below 10%. From the plots in Figure 7, it seems that orbit altitude does not affect propulsive performances in a significant way. However, it should be noted that the focus of this study is on the chemistry of the propellants, specifically their air concentrations. As a result, the analysis presented only considers a constant inflow, and the actual values may vary depending on the specific orbit being considered. Nonetheless, what can be gleaned from the Figure is that the propulsive performances of the system do not appear to be significantly impacted by changes in the air concentration.

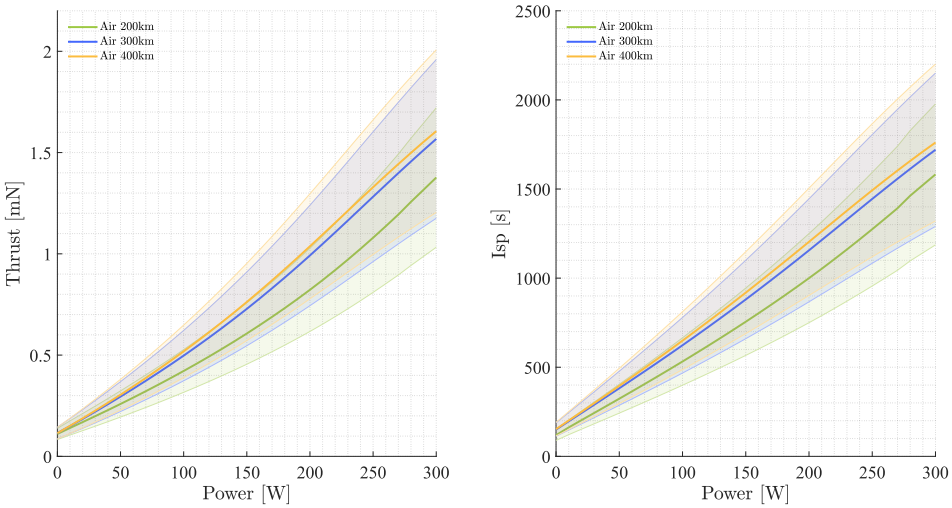


**Figure 7.** Comparison of thrust and specific impulse values obtained from the different propellants with respect to the input power in range 0–300 W.

## 4. Conclusions

In conclusion, this study has examined the chemistry of air as a propellant in a cathodeless thruster using a global model with different input powers and orbit altitudes. The analysis of the steady-value densities has shown that the influences of molecules such as NO, $N_2O$, and $NO_2$ is negligible and that plasma is weakly electronegative under the assumed conditions. In addition, a comparison against xenon and iodine data has been performed. Based on the preliminary estimation of thrust and specific impulse, which covered a range of 0 to 50 W, it has been found that the air case exhibited poor propulsive performances. In fact, its values are only around 50% of those obtained from xenon and iodine data. This discrepancy can be explained by the very low ionization ratio observed at low input power, which was determined to be just 8%. To better understand the chemistry of air, the power range has been increased. Good values of ionization ratios can be achieved around 700 W, where the number of positive ions is almost 76% of the overall particles. Hence, in order to be able to compensate for atmospheric drag, the input power needs to be much higher than the range that was evaluated.

Finally, an analysis has been carried out to investigate the impact of orbit altitude on propulsive performance. To examine the air chemistry, the study considered different concentrations of various species in the inflow of the system. The results have shown that the effects of these factors are constrained within a range of 10% at orbit altitudes of 200 km, 300 km, and 400 km. However, it should be noted that, in this work, the mass inflow was assumed to be constant. Further analysis would be necessary to fully evaluate the impact of orbit altitude on propulsive performances, especially considering that mass inflow is likely to vary with the orbit altitude. Moreover, the influence of ionized particles in the air inflow should be investigated.

**Author Contributions:** Conceptualization, S.D.F., N.S., M.M., R.A., E.C. and F.P.; Methodology, S.D.F., N.S., M.M., R.A., E.C. and F.P.; Software, S.D.F., N.S., M.M., R.A., E.C. and F.P.; Validation, S.D.F., N.S., M.M., R.A., E.C. and F.P.; Formal analysis, S.D.F., N.S., M.M., R.A., E.C. and F.P.; Investigation, S.D.F., N.S., M.M., R.A., E.C. and F.P.; Writing—original draft, S.D.F., N.S., M.M., R.A., E.C. and F.P.; Writing—review & editing, N.S., M.M., R.A., E.C. and F.P.; Visualization, N.S., M.M., E.C. and F.P.; Supervision, N.S., M.M., E.C. and F.P.; Project administration, F.P. All authors have read and agreed to the published version of the manuscript.

**Funding:** This research received no external funding.

**Data Availability Statement:** The data presented in this study are available on reasonable request from the corresponding author.

**Conflicts of Interest:** The authors declare no conflict of interest.

## Appendix A. Atmosphere-Breathing Summarized Chemical Reactions

Table A1 summarizes the 177 chemical reactions considered in the global model. The Table presents the interactions with generic particles denoted as "A" and "B", along with the involved species and reaction rates. Excited species, positive ions and negative ions are respectively indicated with *,$^+$ and $^-$.

**Table A1.** Complete set of considered reactions.

| # | Name | Reaction | Involved Species | Reaction Rates |
|---|---|---|---|---|
| 1 | Atomic Elastic Scattering | $e + A \longrightarrow A + e$ | N, O, $N^+$,$O^+$ | [9,11,51] |
| 2 | Atomic Excitation | $e + A \longrightarrow A^* + e$ | N, O | [9,11] |
| 3 | Atomic Ionization | $e + A \longrightarrow A^+ + 2e$ | N, O | [11,51] |
| 4 | Atomic Neutralization | $e + A^+ \longrightarrow A$ | N, O | [11] |
| 5 | Atomic Attachment | $e + A \longrightarrow A^-$ | $O_2$, NO, $NO_2$ | [11] |
| 6 | Molecular Elastic Scattering | $e + AB \longrightarrow AB + e$ | $N_2$, $O_2$ | [11] |
| 7 | Molecular Excitation | $e + AB \longrightarrow AB^* + e$ | $N_2$ | [11] |
| 8 | Molecular Ionization | $e + AB \longrightarrow AB^+ + 2e$ | $N_2$, $O_2$ | [11] |
| 9 | Molecular Dissociative Ionization | $e + AB \longrightarrow A + B^+ + 2e$ | $O_2$ | [11] |
| 10 | Molecular Dissociative Attachment | $e + AB \longrightarrow A + B^-$ | $O_2$, $NO_2$, $N_2O$ | [11,51] |
| 11 | Molecular Dissociation | $e + AB \longrightarrow A + B + e$ | $N_2$, $O_2$ | [9,11] |
| 12 | Molecular Neutralization | $e + AB^+ \longrightarrow AB$ | $N_2$, $O_2$, NO | [11] |
| 13 | Molecular Attachment | $e + AB \longrightarrow AB^-$ | $O_2$, NO, $NO_2$ | [11] |
| 14 | Molecular Dissociative Neutralization | $e + AB^+ \longrightarrow A + B$ | $N_2$, $O_2$, NO, $NO_2$, $N_2O$ | [11] |
| 15 | Charge Exchange | $A^+ + B \longrightarrow A + B^+$ | N, $N_2$, O, $O_2$, NO, $NO_2$, $N_2O$ | [11] |
| 16 | Mutual Neutralization | $A^+ + B^- \longrightarrow A + B$ | N, $N_2$, O, $O_2$, NO, $NO_2$, $N_2O$ | [11] |
| 17 | Recombination | $A + B \longrightarrow AB$ | N, $N_2$, O, $O_2$, NO | [11] |
| 18 | Ion recombination | $A + B^+ \longrightarrow AB^+$ | N, O, NO | [11] |
| 19 | Associative Detachment | $A + B^- \longrightarrow AB + e$ | O, $O_2$, NO, $NO_2$ | [11] |
| 20 | Associative Neutralization | $A^+ + B^- \longrightarrow AB$ | N, $N_2$, O, $O_2$, NO | [11] |

## References


1. Vaidya, S.; Traub, C.; Romano, F.; Herdrich, G.; Chan, Y.A.; Fasoulas, S.; Roberts, P.; Crisp, N.; Edmondson, S.; Haigh, S.; et al. Development and analysis of novel mission scenarios based on Atmosphere-Breathing Electric Propulsion (ABEP). *CEAS Space J.* **2022**, *14*, 689–706. [CrossRef]
2. Andreussi, T.; Ferrato, E.; Giannetti, V.; Piragino, A.; Paissoni, C.A.; Cifali, G.; Andrenucci, M., Development Status and Way Forward of SITAEL's Air-breathing Electric Propulsion Engine. In Proceedings of the AIAA Propulsion and Energy 2019 Forum, Indianapolis, IN, USA, 19–22 August 2019.
3. Crisp, N.; Roberts, P.; Livadiotti, S.; Oiko, V.; Edmondson, S.; Haigh, S.; Huyton, C.; Sinpetru, L.; Smith, K.; Worrall, S.; et al. The benefits of very low earth orbit for earth observation missions. *Prog. Aerosp. Sci.* **2020**, *117*, 100619. [CrossRef]
4. Virgili-Llop, J.; Roberts, P.; Hao, Z.; Ramio, L.; Beauplet, V. Very Low Earth Orbit mission concepts for Earth Observation. Benefits and challenges. In Proceedings of the Reinventing Space Conference, London, UK, 18–21 November 2014.
5. Fujita, K.; Noda, A., Rarefied Aerodynamics of a Super Low Altitude Test Satellite. In Proceedings of the 41st AIAA Thermophysics Conference, San Antonio, TX, USA, 22–25 June 2009.
6. Schönherr, T.; Komurasaki, K.; Romano, F.; Massuti-Ballester, B.; Herdrich, G. Analysis of Atmosphere-Breathing Electric Propulsion. *IEEE Trans. Plasma Sci.* **2015**, *43*, 287–294. [CrossRef]
7. Souhair, N.; Magarotto, M.; Majorana, E.; Ponti, F.; Pavarin, D. Development of a lumping methodology for the analysis of the excited states in plasma discharges operated with argon, neon, krypton, and xenon. *Phys. Plasmas* **2021**, *28*, 093504,
8. Pekker, L.; Keidar, M. Analysis of Airbreathing Hall-Effect Thrusters. *J. Propuls. Power* **2012**, *28*, 1399–1405. [CrossRef]
9. Zhou, J.; Taccogna, F.; Fajardo, P.; Ahedo, E. Performance analysis of alternative propellants for a helicon plasma thruster. In Proceedings of the 7th Space Propulsion Conference, Estoril, Portugal, 17–19 March 2021
10. Romano, F.; Herdrich, G.; Chan, Y.A.; Crisp, N.; Roberts, P.C.; Holmes, B.E.; Edmondson, S.; Haigh, S.; Macario-Rojes, A.; Oiko, V.T.A.; et al. Design of an intake and a thruster for an atmosphere-breathing electric propulsion system. *CEAS Space J.* **2022**, *14*, 707–715. [CrossRef]
11. Taploo, A.; Lin, L.; Keidar, M. Analysis of ionization in air-breathing plasma thruster. *Phys. Plasmas* **2021**, *28*, 093505. [CrossRef]
12. Grondein, P.; Lafleur, T.; Chabert, P.; Aanesland, A. Global model of an iodine gridded plasma thruster. *Phys. Plasmas* **2016**, *23*, 033514. [CrossRef]
13. Takahashi, K. Thirty percent conversion efficiency from radiofrequency power to thrust energy in a magnetic nozzle plasma thruster. *Sci. Rep.* **2022**, *12*, 18618. [CrossRef]
14. Liou, J.C.; Johnson, N.; Hill, N. Controlling the growth of future LEO debris populations with active debris removal. *Acta Astronaut.* **2010**, *66*, 648–653. .: 10.1016/j.actaastro.2009.08.005. [CrossRef]
15. Di Cara, D.; Gonzalez del Amo, J.; Santovincenzo, A.; Carnicero Domíguez, B.; Arcioni, M.; Caldwell, A.; Roma, I. RAM Electric Propulsion for Low Earth Orbit Operation: An ESA study. In Proceedings of the 30 th International Electric Propulsion Conference, Florence, Italy, 17–20 September 2007.
16. Nishiyama, K. A Study of Air Breathing Ion Engine. *Space Technol. Jpn. Jpn. Soc. Aeronaut. Space Sci.* **2005**, *4*, 21–27. [CrossRef]
17. Tisaev, M.; Ferrato, E.; Giannetti, V.; Paissoni, C.; Baresi, N.; Lucca Fabris, A.; Andreussi, T. Air-breathing electric propulsion: Flight envelope identification and development of control for long-term orbital stability. *Acta Astronaut.* **2022**, *191*, 374–393. [CrossRef]
18. Hohman, K. Atmospheric Breathing Electric Thruster for Planetary Exploration. In Proceedings of the NIAC Spring Symposium, Pasadena, CA, 27–29 March 2012.
19. Romano, F.; Binder, T.; Herdrich, G.H.; Fasoulas, S.; Schönherr, T. Air-Intake Design Investigation for an Air-Breathing Electric Propulsion System. In Proceedings of the 34th International Electric Propulsion Conference, Kobe, Japan, 4–10 July 2015. [CrossRef]
20. Romano, F.; Massuti-Ballester, B.; Binder, T.; Herdrich, G.; Fasoulas, S.; Schönherr, T. System analysis and test-bed for an atmosphere-breathing electric propulsion system using an inductive plasma thruster. *Acta Astronaut.* **2018**, *147*, 114–126. [CrossRef]
21. Mrózek, K.; Dytrych, T.; Moliš, P.; Dániel, V.; Obrusník, A. Global plasma modeling of a magnetized high-frequency plasma source in low-pressure nitrogen and oxygen for air-breathing electric propulsion applications. *Plasma Sources Sci. Technol.* **2021**, *30*, 125007. [CrossRef]
22. Taccogna, F.; Cichocki, F.; Minelli, P. Coupling plasma physics and chemistry in the PIC model of electric propulsion: Application to an air-breathing, low-power Hall thruster. *Front. Phys.* **2022**, *10*, 989. [CrossRef]
23. Bellomo, N.; Manente, M.; Trezzolani, F.; Gloder, A.; Selmo, A.; Mantellato, R.; Toson, E.; Cappellini, L.; Duzzi, M.; Scalzi, D.; et al. Enhancement of microsatellites' mission capabilities: integration of REGULUS electric propulsion module into UniSat-7. In Proceedings of the 70th International Astronautical Congress (IAC), Washington, DC, USA, 21–25 October 2019.
24. Manente, M.; Trezzolani, F.; Magarotto, M.; Fantino, E.; Selmo, A.; Bellomo, N.; Toson, E.; Pavarin, D. REGULUS: A propulsion platform to boost small satellite missions. *Acta Astronaut.* **2019**, *157*, 241–249. [CrossRef]
25. Goebel, D.M.; Katz, I. *Fundamentals of Electric Propulsion: Ion and Hall Thrusters*; John Wiley & Sons, Inc.: Hoboken, NJ, USA, 2008; pp. 1–507. [CrossRef]
26. Magarotto, M.; Di Fede, S.; Souhair, N.; Andrews, S.; Ponti, F. Numerical suite for cathodeless plasma thrusters. *Acta Astronaut.* **2022**, *197*, 126–138. [CrossRef]

27. Souhair, N.; Magarotto, M.; Ponti, F.; Pavarin, D. Analysis of the plasma transport in numerical simulations of Helicon plasma thrusters. *AIP Adv.* **2021**, *11*, 115016. [CrossRef]
28. Majorana, E.; Souhair, N.; Ponti, F.; Magarotto, M. Development of a Plasma Chemistry Model for Helicon Plasma Thruster analysis. *Aerotec. Missili Spaz.* **2021**, *100*, 225–238. [CrossRef]
29. Lieberman, M.A.; Lichtenberg, A.J. *Principles of Plasma Discharges and Materials Processing*, 2nd ed.; Wiley: Hoboken, NJ, USA, 2005.
30. Guaita, M.; Magarotto, M.; Manente, M.; Pavarin, D.; Lavagna, M. Semi-Analytical Model of a Helicon Plasma Thruster. *IEEE Trans. Plasma Sci.* **2022**, *50*, 425–438. [CrossRef]
31. Andrews, S.; Di Fede, S.; Magarotto, M. Fully kinetic model of plasma expansion in a magnetic nozzle. *Plasma Sources Sci. Technol.* **2022**, *31*, 035022. [CrossRef]
32. Lafleur, T.; Habl, L.; Rossi, E.Z.; Rafalskyi, D. Development and validation of an iodine plasma model for gridded ion thrusters. *Plasma Sources Sci. Technol.* **2022**, *31*, 114001. [CrossRef]
33. Chabert, P. An expression for the hl factor in low-pressure electronegative plasma discharges. *Plasma Sources Sci. Technol.* **2016**, *25*, 025010. [CrossRef]
34. Lucken, R.; Marmuse, F.; Tavant, A.; Bourdon, A.; Chabert, P. Global model of a magnetized ion thruster with xenon and iodine. In Proceedings of the 36th International Electric Propulsion Conference, Vienna, Austria, 15–20 September 2019; Number IEPC-2019-678.
35. Thorsteinsson, E.G.; Gudmundsson, J.T. A global (volume averaged) model of a chlorine discharge. *Plasma Sources Sci. Technol.* **2009**, *19*, 015001. [CrossRef]
36. Brokaw, R.S. Predicting Transport Properties of Dilute Gases. *Ind. Eng. Chem. Process. Des. Dev.* **1969**, *8*, 240–253.
37. Souhair, N.; Magarotto, M.; Dalle Fabbriche, S.; Andriulli, R.; Andrews, S.; Ponti, F.; Pavarin, D. Simulation and modelling of an iodine fed Helicon Plasma Thruster. In Proceedings of the 37th International Electric Propulsion Conference, Cambridge, MA, USA, 19–23 June 2022; Number IEPC-2022-496.
38. MSIS-E-90 Atmosphere Model. Available online: https://ccmc.gsfc.nasa.gov/modelweb/models/msis_vitmo.php (accessed on 10 October 2022).
39. Hagelaar, G.J.; Pitchford, L.C. Solving the Boltzmann equation to obtain electron transport coefficients and rate coefficients for fluid models. *Plasma Sources Sci. Technol.* **2005**, *14*, 722–733. [CrossRef]
40. Berenguer, C.; Katsonis, K.; Gonzalez del Amo, J. Using of an Iodine Detailed Global Model for Characterization and for Optical Diagnostics of Helicon Thrusters. In Proceedings of the 6th Space Propulsion Conference, Seville, Spain, 14–18 May 2018. [CrossRef]
41. Lafleur, T. Helicon plasma thruster discharge model. *Phys. Plasmas* **2014**, *21*, 043507,
42. Bittencourt, J.A. *Fundamentals of Plasma Physics*; Springer: New York, NY, USA, 2004. [CrossRef]
43. Lafleur, T.; Charles, C.; Boswell, R.W. Electron temperature characterization and power balance in a low magnetic field helicon mode. *J. Phys. D Appl. Phys.* **2011**, *44*, 185204. [CrossRef]
44. Magarotto, M.; Pavarin, D. Parametric Study of a Cathode-Less Radio Frequency Thruster. *IEEE Trans. Plasma Sci.* **2020**, *48*, 2723–2735. [CrossRef]
45. Sutton, G.; Biblarz, O. *Rocket Propulsion Elements*; A Wiley Interscience Publication; Wiley: Hoboken, NJ, USA, 2001.
46. Bellomo, N.; Magarotto, M.; Manente, M.; Trezzolani, F.; Mantellato, R.; Cappellini, L.; Paulon, D.; Selmo, A.; Scalzi, D.; Minute, M.; et al. Design and In-orbit Demonstration of REGULUS, an Iodine electric propulsion system. *CEAS Space J.* **2021**, *14*, 79-90. [CrossRef]
47. Manente, M.; Trezzolani, F.; Mantellato, R.; Scalzi, D.; Schiavon, A.; Souhair, N.; Duzzi, M.; Cappellini, L.; Barbato, A.; Paulon, D.; et al. REGULUS: Iodine Fed Plasma Propulsion System for Small Satellites. In Proceedings of the 36th International Electric Propulsion Conference, Vienna, Austria, 15–20 September 2019; Number IEPC-2019-417,
48. Magarotto, M.; Melazzi, D.; Pavarin, D. 3D-VIRTUS: Equilibrium condition solver of radio-frequency magnetized plasma discharges for space applications. *Comput. Phys. Commun.* **2020**, *247*, 106953. [CrossRef]
49. Shabshelowitz, A. Study of RF Plasma Technology Applied to Air-Breathing Electric Propulsion. Ph.D. Thesis, University of Michigan, Ann Arbor, MI, USA, 2013.
50. CRC Handbook. *CRC Handbook of Chemistry and Physics*, 88th ed.; CRC Press: Boca Raton, FL, USA, 2007.
51. LXcat, The Plasma Data Exchange Project. Available online: https://nl.lxcat.net (accessed on 2 September 2022).